

Hamiltonian non-Hermiticity: accurate dynamics with the multiple Davydov D_2 Ansätze

Lixing Zhang^{1,2}, Kaijun Shen¹, Yiying Yan³, Kewei Sun⁴, Maxim F. Gelin⁴, and Yang Zhao¹

¹*School of Materials Science and Engineering, Nanyang Technological University, Singapore 639798, Singapore*

²*Department of Chemistry and Biochemistry, University of California Los Angeles, Los Angeles, CA 90095, USA*

³*School of Science, Zhejiang University of Science and Technology, Hangzhou 310023, China*

⁴*School of Science, Hangzhou Dianzi University, Hangzhou 310018, China*

(Dated: October 17, 2024)

We examine the applicability of the numerically accurate method of time dependent variation with multiple Davydov Ansätze (mDA) to non-Hermitian systems. Three systems of interest includes: a non-Hermitian system of dissipative Landau-Zener transitions, a non-Hermitian, multimode Jaynes-Cummings model, and a dissipative Holstein-Tavis-Cummings model, where complex many-body dynamics are accurately captured by the mDA method. Our findings highlight the versatility of the mDA as a powerful numerical tool for investigating complex many-body non-Hermitian systems, which can be extended to explore diverse phenomena such as skin effects, excited-state dynamics, and spectral topology in the non-Hermitian field.

I. INTRODUCTION

The unconventional realm of non-Hermitian physics [1–4], stemming from a novel, mainly phenomenological framework of addressing quantum open-system dynamics, offers an alternative avenue for investigating the behaviors of open quantum systems and the fascinating topic of quantum dissipation. Non-Hermitian physics has spawned many novel phenomena, such as complicated bandgap definition [5–7], topological phase transition [8–13], bulk-boundary correspondence [14, 15], and non-Hermitian skin effect [16–20]. On the other hand, the description of various decoherence and lifetime processes in terms of non-Hermitian Hamiltonians has long been a method of choice in photophysics and spectroscopy[21] and, furthermore, the effective non-Hermitian Hamiltonians can be constructed for driven quantum systems [22]

Traditional approaches to quantum physics often assume isolation, where fundamental principles are based on the premise that the object of interest operates in a closed system without interactions with the environment. The energy operator of a quantum closed system is typically described by a Hermitian operator known as a Hamiltonian, represented by a Hermitian matrix. This depiction simplifies the physical model and highlights the conservation of energy within the system. However, in reality, many physical systems are open and susceptible to environmental influences.

While various methods exist to incorporate bath effects in the system dynamics, the non-Hermitian approach is unique in the semi-empirical manner in which it disrupts the well-known Hamiltonian hermiticity in integrating environmental influences [23, 24]. Consequently, a novel formalism based on non-Hermitian Hamiltonians brings about energy and particle number non-conservation. Dissipation, stemming from environmental effects, stands out as a prevalent and inevitable consequence.

In various fields, dissipation is typically viewed as a

negative effect, as it often diminishes the functionality of devices used for sensing, computation, and communication. However, non-Hermitian physics challenges this perspective by revealing unconventional physical effects associated with dissipation or a strategic interplay of dissipation and amplification. Particularly in open systems with gain or loss, the unique properties of non-conserved energy and non-unitary evolution result in complex eigenvalues and introduce exotic features to the eigenstates of the systems.

One important application of non-Hermitian Hamiltonians is represented by cavity quantum electrodynamics (QED) [25], where cavity photon dissipation is modeled by adopting a complex photon frequency [26]. In cavity materials science, the interaction between light and matter inside optical cavities leads to the formation of polaritonic states, which are hybrid states combining photonic and excitonic (matter) components. In a realistic experimental setup, cavity photons have a finite lifetime inside the cavity, leading to dissipative effects that are inherently non-Hermitian. To accurately describe these systems, one can phenomenologically incorporate various sources of dissipation into a non-Hermitian Hamiltonian, responsible for spectroscopic broadening of the light-matter eigenspectrum. Strong coupling in cavity QED is commonly defined when the matter-cavity coupling strength g_c is much larger than the cavity loss rate κ (assuming the matter de-excitation rate is much smaller than κ). Under these conditions, cavity loss described by the non-Hermitian Hamiltonian plays a significant role in the system's dynamics and influences polariton photochemistry significantly [27–30].

Recent investigations into non-Hermitian Hamiltonians have revealed significant effects of cavity loss on polaritonic dynamics. One notable impact is the reduction of excited-state populations with photonic character, which alters the behavior of polaritonic states [31]. Additionally, cavity loss can enhance the rates of photochemical reactions [32] and protect molecules from photodam-

age by decreasing the time photoexcited molecules spend in nuclear configurations prone to damage [33]. However, when multiple excitation manifolds are accessible, the influence of cavity loss becomes more complex [34]. This complexity underscores the need for detailed, accurate calculations of non-Hermitian dynamics to optimize cavity parameters for controlling photochemical reactions.

Time dependent variation with multiple Davydov Ansatz (mDA) is an accurate method to unveil the dynamics of a complex many-body quantum system by solving the time-dependent Schrödinger equation (TDSE) numerically “exactly” [35, 36]. By expressing the bosonic part of the wave function with an overcomplete basis of coherent-state superpositions, mDA can capture the intricate dynamics for all multi-species bosonic degrees of freedom (DOF). Moreover, in the mDA algorithm, computational complexity only scales linearly with respect to the number of bosonic DOFs, which further empowers mDA to be highly adaptive to a diverse array of systems. For examples, mDA has been successfully applied to a variety of systems in chemical physics, condensed matter physics, cavity QED, nonlinear spectroscopy and many-body quantum dynamics [37–42].

Despite the success of mDA in Hermitian systems, till date, it has not yet been adopted in the novel regime of non-Hermitian systems. In the remainder of this paper, we showcase the application of mDA to three particular non-Hermitian systems of interest. The first is a dissipative Landau-Zener (LZ) system with a tunable non-Hermitian term. Proven by the Kibble-Zurek theory [43], the non-Hermitian effects in the LZ system is related to various of parameters including relaxation time, temperature and quenching time. The second is a non-Hermitian, multimode Jaynes-Cummings (JC) model, which usually describes a two-level system interacting with lossy cavities or waveguides [44–46]. In the third case, we use a non-Hermitian term to describe realistic experimental environment in a dissipative Holstein-Tavis-Cummings (HTC) model, which is a model that describes, e.g., cavity singlet fission processes with Kerr effect. In addition, we benchmark the results generated by mDA against numerically exact solutions.

II. METHODOLOGY

A. The multi-D₂ Ansatz and the Time Dependent Variational Principle

The governing equation for the time evolution of quantum systems, the TDSE can be written as follow:

$$i \frac{\partial}{\partial t} |\Psi(t)\rangle = \hat{H} |\Psi(t)\rangle \quad (1)$$

For non-Hermitian systems, the left ($\langle\langle n|$) and right ($|n\rangle\rangle$) eigenstates of the Hamiltonian are not Hermitian

conjugates. This leads to differences in the time evolution of $\langle\langle \Psi(t)|$ and $|\Psi(t)\rangle$ (i.e. $\langle\langle \Psi(t)| \neq |\Psi(t)\rangle^\dagger$). In this paper, we only focus on the time evolution $|\Psi(t)\rangle$.

For complex systems, the complete solution of TDSE is almost impossible to obtain. Therefore, we employ the multiple Davydov D₂ (mD2) Ansatz, also known as the multi-D₂ Ansatz, to variationally solve the TDSE. For the three systems considered in this work, the mD2 Ansatz can be written as:

$$|D_2^M(t)\rangle = \sum_s^{N_s} |s\rangle \left[\sum_{n=1}^M A_{ns}(t) \exp\left[\left(\sum_k^{N_b} \alpha_{nk}(t) b_k^\dagger - \text{H.c.}\right)\right] |\{0_k\}\rangle \right] \quad (2)$$

Here, N_s is the total number of spin DOF, and $|s\rangle$ represents a spin state with spin s . Similarly, N_b is the total number of bosonic DOF, and $|\{0_k\}\rangle$ is the multi-mode vacuum state. The multiplicity M is the number of single D₂ Ansatz in the mD2 Ansatz. Each single D₂ Ansatz is characterized by a group of independent variational parameters: amplitude $A_{ns}(t)$ and displacement $\alpha_{nk}(t)$. This expresses the boson part of the wavefunctions through a linear combination of coherent states that have different displacements. They form an overcomplete basis that is capable of reproducing accurate boson dynamics at sufficiently large M .

Following the Lagrange’s principle, the Ansatz can be used to solve the TDSE variationally. We construct the Lagrangian in the following form ($\hbar = 1$) [47–49]:

$$L = \langle D_2^M(t) | \left(\frac{d}{dt} + i\hat{H} \right) | D_2^M(t) \rangle \quad (3)$$

To obtain the time trajectory of the variational parameters, the action functional $S = \int_{t_1}^{t_2} L dt$ should be minimized. This can be enforced by the Euler-Lagrange (EL) equation:

$$\frac{d}{dt} \frac{\partial L}{\partial \dot{u}_n^*} - \frac{\partial L}{\partial u_n^*} = 0, \quad u_n \in [A_{ns}, \alpha_{nk}] \quad (4)$$

This yields the equation of motions (EOMs), which are a set of coupled differential equations. The EOMs can be solved via the 4th order Runge-Kutta method.

B. Observables

For an arbitrary operator Q , its expectation value in the mD2 basis can be written as:

$$\langle \tilde{Q} \rangle(t) = \langle D_2^M(t) | Q | D_2^M(t) \rangle \quad (5)$$

When \hat{H} is non-Hermitian, the time evolution becomes non-unitary. This is characterized by a non-unitary normalization factor, which can be written as:

$$N_f(t) = \langle D_2^M(t) | D_2^M(t) \rangle = \sum_{m,n}^M \sum_s^{N_s} A_{ms}^*(t) A_{ns}(t) S_{mn} \quad (6)$$

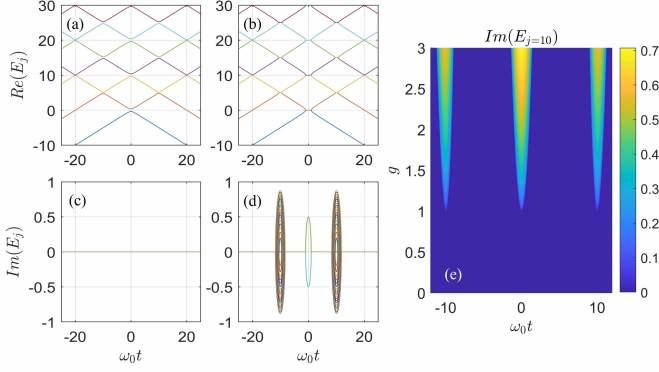


Figure 1. The eigenvalues of \hat{H} with $N = 1$ and the \mathcal{PT} transition. (a) and (c): The real and imaginary part of the eigenvalues when $g=0.5$. (b) and (d): The real and imaginary part of the eigenvalues when $g=2$. (e): Contour plot illustrating the maximum imaginary part of the eigenvalues over time and g . A distinct demarcation is noticeable at $g = 1$. Remaining parameters are as follows: $v = 0.5\omega_0^2$, $\lambda = 0.2\omega_0$, $\omega = 10\omega_0$ and $\Delta = 0.5\omega_0$ (ω_0 is the unit frequency).

with:

$$S_{mn} = \exp \left[\sum_k^{N_b} \alpha_{mk}^* \alpha_{nk} - \frac{1}{2} (|\alpha_{mk}|^2 + |\alpha_{nk}|^2) \right] \quad (7)$$

III. RESULTS AND DISCUSSION

A. Dynamics of the non-Hermitian LZ transitions

A non-Hermitian LZ transition may be described by a non-Hermitian Hamiltonian as follows:

$$\hat{H}_{\text{NLZ}} = \begin{bmatrix} vt/2 & \Delta \\ \Delta(1-g) & -vt/2 \end{bmatrix} \quad (8)$$

where v is the scanning velocity, Δ is the tunneling strength between two levels, and g is the strength of non-Hermitian level coupling. In particular, when $g = 0$, the Hermitian LZ problem is recovered.

In addition to the non-Hermitian coupling of electronic DOFs, we also consider the non-Hermitian interaction between spin and an Ohmic heat bath. The Hamiltonian for the total system can be written as:

$$\hat{H} = \hat{H}_{\text{NLZ}} + \sum_k^{N_b} \omega_k \hat{b}_k^\dagger \hat{b}_k + \begin{bmatrix} 0 & 1 \\ 1-g & 0 \end{bmatrix} \sum_k^{N_b} \frac{\lambda_k}{2} (\hat{b}_k^\dagger + \hat{b}_k) \quad (9)$$

Here, \hat{b}_k^\dagger (\hat{b}_k) is the creation(annihilation) operator of the k^{th} mode of the quantum bath. With a total number of N_b bath modes, ω_k and λ_k are the frequencies and the coupling strengths of the k^{th} mode, respectively. The

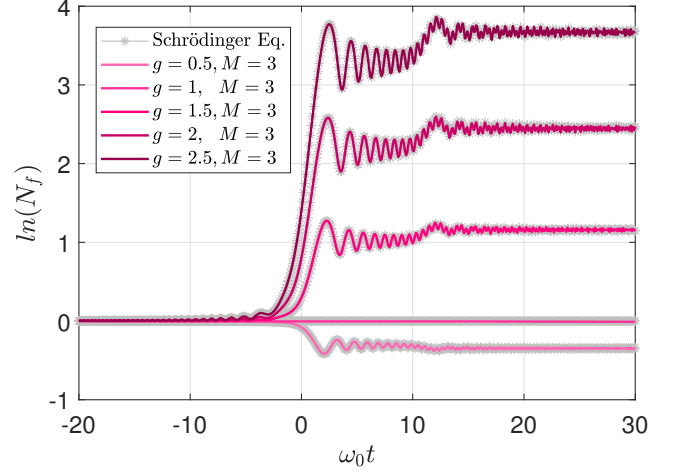


Figure 2. Time evolution of the norm of the wavefunction calculated by the TDSE(dotted grey line) and mD2(red line, deeper colors represent higher magnitude of g) when g is changed from 0.5 to 2.5. The rest of the parameters are set as: $\Delta = 0.5\omega_0$, $\lambda = 0.2\omega_0$, $\omega = 10\omega_0$, and $v = 0.5\omega_0^2$.

bath modes are characterized by an Ohmic-type spectral density function:

$$J(\omega) = \sum_k^{N_b} (\lambda_k)^2 \delta(\omega - \omega_k) = 2\alpha\omega e^{-\omega/\omega_c} \quad (10)$$

where α is the strength of spin-bath coupling, and ω_c is the cut-off frequency.

To get a physical picture of the problem, we first investigate the energy spectrum of \hat{H} when $N_b = 1$. In Fig. 1, we present the effect of the non-Hermitian term g on the energy spectrum of the problem. The magnitude of g separates the problem into two phases marked by the emergence of imaginary eigenvalues. When $g = 0.5$, notwithstanding \hat{H} becomes non-Hermitian, its eigenvalues, as depicted in Fig. 1(a) and (c), are real across all time points, while the renowned avoided crossings remain observable. However, when $g = 2$, as shown in Fig. 1(b) and (d), while the energy spectrum remains predominantly real across most time points, complex eigenvalues emerge as energy levels intersect, supplanting the previously observed avoided crossings. In Fig. 1(e), by plotting the maximum imaginary eigenvalue with respect to time and g , it becomes evident that the transition point between these two cases is marked by $g = 1$, which is known as the Exceptional Point(EP). When $g < 1$, the eigenvalues of \hat{H} remain real at any time points, thus preserving the parity-time (\mathcal{PT}) symmetry. Conversely, for $g > 1$, complex eigenvalues emerge, leading to the breakdown of the $\mathcal{P} - \mathcal{T}$ symmetry.

We note that for both \mathcal{PT} -preserved and \mathcal{PT} -broken phase, the mD2 Ansatz remains numerically accurate. To compare the results produced by the mD2 Ansatz and by solving the TDSE, in Fig. 2, we consider $N = 1$

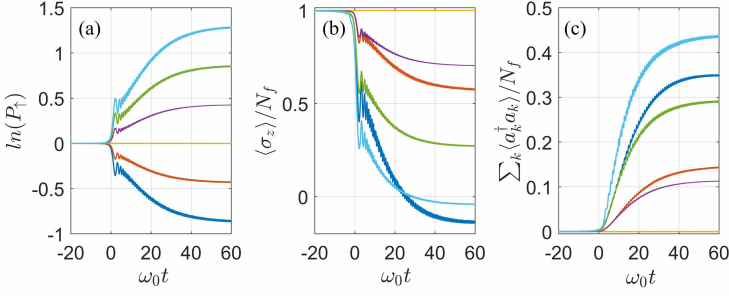


Figure 3. Time evolution of different observables calculated by mD2 with $M=5$. Different colors of lines indicate different magnitudes of g : navy blue: $g=0$; red: $g=0.5$; yellow: $g=1$; purple: $g=1.5$; green: $g=2$; sky blue: $g=2.5$ (a). Time evolution of the unnormalized upper-state population in logarithmic scale. (b). Time evolution of the normalized spin polarization. (c). Time evolution of the total bath phonon number. The rest of the parameters are set as: $\Delta = 0.5\omega_0$, $\lambda = 0.2\omega_0$, $\omega = 10\omega_0$, and $v = 0.5\omega_0^2$.

and plot the normalization factor N_f against time in logarithmic scale across a range of values for g spanning from 0.5 to 2.5. The colored lines (mD2 Ansatz with $M=3$) completely overlap with the grey dotted lines (TDSE), hence the validity of the mD2 Ansatz is confirmed for non-Hermitian systems. Notably, at EP where $g = 1$, N_f remains unitary throughout the evolution. Unlike the unitary evolutions in Hermitian physics, this phenomenon arises from the absence of tunneling strength between $|\uparrow\rangle$ and $|\downarrow\rangle$. With the system initialized on $|\uparrow\rangle$, the wave function remains invariant throughout the evolution.

To further examine the applicability of the mD2 Ansatz in more complicated systems, in Fig. 3, we increase N_b to 60, and showcase the time evolution of various observables across different strengths of non-Hermitian level coupling calculated by the mD2 Ansatz. While the parameters $\Delta = 0.2\omega_0$, $\alpha = 0.002$, and $\omega_c = 10\omega_0$ are held constant, the parameter g is varied from 0 to 2.5 across three different regimes: the Hermitian regime, the \mathcal{PT} -preserved regime, and the \mathcal{PT} -broken regime. In Fig. 3a, the time evolution of the unnormalized population is presented in logarithmic scale. Clearly, $P_\uparrow(t)$ increases with g monotonically. The origin of such phenomenon arises from the non-Hermitian nature of the Hamiltonian, which exists in all three regimes regardless of the \mathcal{PT} symmetry. In Fig. 3b and Fig. 3c, we plot the time evolution of normalized observables, which are obtained by dividing the expectation value of unnormalized observables by the norm of the wavefunction. In the \mathcal{PT} -preserved regime ($g = 0, 0.5$, and 1), an increase in g leads to a decrease in both the normalized spin polarization ($\langle\sigma_z\rangle/N_f$) and the total phonon number of the bath ($\sum_k \langle a_k^\dagger a_k \rangle / N_f$). This suggests that the effect of non-Hermiticity in this regime can be roughly interpreted as a reduction in the effective spin-bath coupling strength. Similarly, in the \mathcal{PT} -broken regime ($g = 1.5, 2$, and 2.5),

an increase in g results in an increase in both the normalized spin polarization and the total phonon number of the bath, implying an increase in the effective spin-bath coupling strength. Furthermore, a noticeable change in the gradient of the lines can be observed in Fig. 3b. This indicates that strength of the non-Hermitian level coupling also changes the effective spin-bath coupling.

B. Dynamics of the non-Hermitian multi-mode JC model

Our next model to consider is a non-Hermitian version of the much-studied, paradigmatic JC model. The Hamiltonian of a non-Hermitian, multimode JC model reads

$$H = \frac{1}{2}\omega_0\hat{\sigma}_z - \frac{i\gamma}{2}\hat{\sigma}_+\hat{\sigma}_- + \sum_k \left(\omega_k - \frac{i\kappa_k}{2} \right) \hat{a}_k^\dagger \hat{a}_k + \sum_k \frac{g_k}{2} (\hat{\sigma}_- \hat{a}_k^\dagger + \hat{\sigma}_+ \hat{a}_k) \quad (11)$$

where \hat{a}_k^\dagger (\hat{a}_k) represents the creation (annihilation) operator for the k -th mode of cavity, and $\hat{\sigma}^+ = |e\rangle\langle g|$ ($\hat{\sigma}^- = |g\rangle\langle e|$) are the raising (lowering) Pauli operators. ω_0 is the transition frequency of the two-level system. ω_k are the frequencies of cavity modes. γ and κ_k denote the decay rates of the excited state of the two-level system and the cavity modes, respectively. Time evolution of this model can be exactly solved due to its symmetry, which conserves the total excitation number $\hat{N}_e = \hat{\sigma}_+\hat{\sigma}_- + \sum_k \hat{a}_k^\dagger \hat{a}_k$, and thus provides an ideal testbed to check the accuracy of the present variational approach. We consider a single-excitation subspace in which the time evolution can be described by the following Ansatz

$$|\Psi(t)\rangle = c_e(t)|e, \{0_k\}\rangle + \sum_k c_{gk}(t)|g, \{1_k\}\rangle. \quad (12)$$

Here $c_e(t)$ and $c_{gk}(t)$ are the probability amplitudes. $|e, \{0_k\}\rangle = |e\rangle \otimes |\{0_k\}\rangle$ and $|g, \{1_k\}\rangle = |g\rangle \otimes |\{1_k\}\rangle$ where $|e\rangle$ and $|g\rangle$ are the excited and ground states of the two-level system, respectively. $|\{0_k\}\rangle$ is the multi-mode vacuum state and $|\{1_k\}\rangle$ implies that one photon occupies the mode k and the remaining modes are empty. From the TDSE, we obtain EOMs for the coefficients:

$$i\frac{d}{dt}c_e(t) = \frac{\omega_0 - i\gamma}{2}c_e(t) + \sum_k \frac{g_k}{2}c_{gk}(t), \quad (13)$$

$$i\frac{d}{dt}c_{gk}(t) = \left(\omega_k - \frac{\omega_0}{2} - i\frac{\kappa_k}{2} \right) c_{gk}(t) + \frac{g_k}{2}c_e(t). \quad (14)$$

Provided $|\Psi(0)\rangle = |e, \{0_k\}\rangle$, the EOMs can be numerically solved and the population of the excited state of the two-level system can be computed as

$$P_e(t) = \frac{|c_e(t)|^2}{|c_e(t)|^2 + \sum_k |c_{gk}(t)|^2} \quad (15)$$

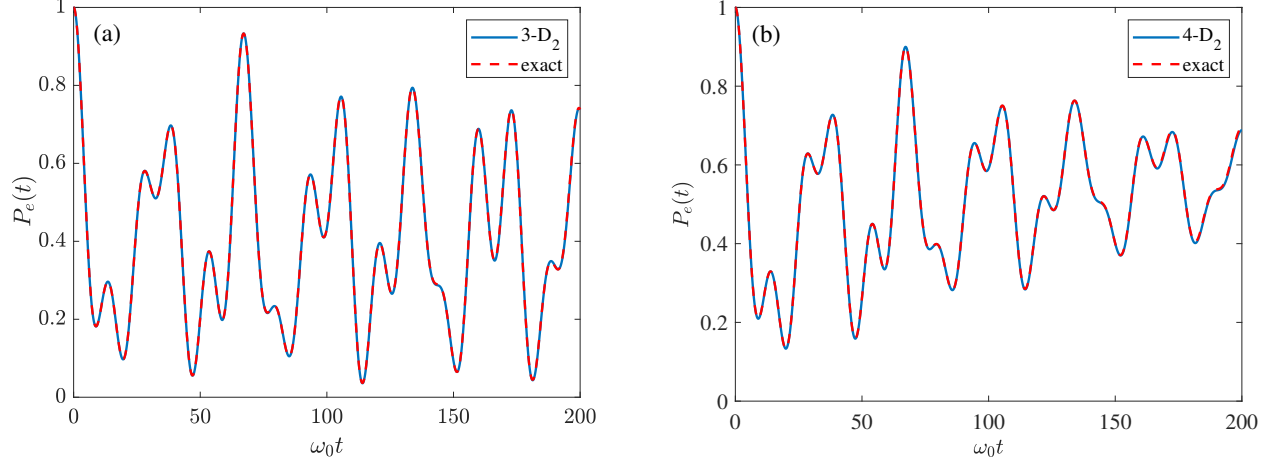


Figure 4. Excited-state population versus time calculated by the mD2(blue line) and TDSE(dashed red line) for $N_b = 3$, $\omega_k/\omega_0 = (1.0, 1.2, 1.3)$, $g_k = 0.2\omega_0$, $\gamma = 10^{-2}\omega_0$, and (a) $\kappa_k = \gamma$, and (b) $\kappa_k = 5\gamma$. Ansatz multiplicity $M = 3$ and 4 in the left and right panel, respectively.

This is referred to as a numerically exact solution and is used to benchmark the variational results.

Figure 4 showcases the comparison between the numerically exact and variational solutions for $N_b = 3$, $g_k = 0.2\omega_0$, $\omega_k/\omega_0 = (1.0, 1.2, 1.3)$, $\gamma = 10^{-2}\omega_0$, and two sets of κ_k . The mD2 Ansatz multiplicity, M , is 3 and 4 in the left and right panel of Fig. 4, respectively. We see that the variational results are in perfect agreement with the numerically exact results, confirming the validity of the variational approach. We have verified that the variational results coincide with the numerically exact solutions of the non-Hermitian JC model ranging from the single to multi-mode case in a broad range of parameters. These findings suggest that the variational approach is capable of solving TDSE governed by a non-Hermitian Hamiltonian.

C. Dynamics of population decay in the non-Hermitian HTC model

The HTC model is coined by augmenting the Tavis-Cummings (TC) model with a bath of phonon modes[50]. The HTC model has been extensively employed in describing many-body quantum dynamics in various molecular cavity QED systems [51, 52]. The Hamiltonian of the HTC model can be written as

$$\hat{H}_{\text{HTC}} = \hat{H}_{\text{TC}} + \hat{H}_{\text{R}} + \hat{H}_{\text{I}}, \quad (16)$$

where \hat{H}_{R} is the reservoir Hamiltonian, \hat{H}_{I} is the interaction Hamiltonian of the reservoir and the TC model, and \hat{H}_{TC} is the Hamiltonian of the TC model, consisting

of N two-level atoms and one cavity-mode, which reads

$$\hat{H}_{\text{TC}} = \omega_c \hat{a}^\dagger \hat{a} + \sum_{n=1}^N [\omega_n \hat{\sigma}_n^+ \hat{\sigma}_n^- + \frac{\omega_{\text{R}}}{\sqrt{N}} (\hat{a}^\dagger \hat{\sigma}_n^- + \hat{a} \hat{\sigma}_n^+)]. \quad (17)$$

Here, ω_c is the frequency of cavity mode, and ω_n is the transition frequency of the n th qubit. For simplicity, we set $\omega_n = \omega_0$. The qubit-cavity coupling is assumed to be $\omega_{\text{R}}/\sqrt{N}$. The reservoir Hamiltonian \hat{H}_{R} takes the form

$$\hat{H}_{\text{R}} = \sum_k \omega_k \hat{b}_k^\dagger \hat{b}_k, \quad (18)$$

and the qubit-reservoir interaction Hamiltonian

$$\hat{H}_{\text{I}} = -\frac{\lambda}{\sqrt{N}} \sum_k \sum_{n=1}^N \omega_k \hat{\sigma}_n^+ \hat{\sigma}_n^- (e^{-ikn} \hat{b}_k^\dagger + e^{ikn} \hat{b}_k). \quad (19)$$

Here, only the diagonal qubit-reservoir coupling strength λ is considered, and a linear phonon dispersion is assumed:

$$\omega_k = \omega_{k0} [1 + \Omega (\frac{2|k|}{\pi} - 1)], \quad (20)$$

where ω_{k0} denotes the central energy of the phonon band, $\Omega \in [0, 1]$ is the band width, and the momentum is set to be $k = 2\pi l/N$ with $(l = -\frac{N}{2} + 1, \dots, \frac{N}{2})$.

The Hamiltonian in Eq. (17) is Hermitian. To take into account various dissipative effects that are not included in the reservoir Hamiltonian \hat{H}_{R} , such as cavity loss, a non-Hermitian term,

$$\hat{H}_{\text{NH}} = -i\kappa |g, \{1\}\rangle \langle g, \{1\}|, \quad (21)$$

can be added to Eq. (17), where κ is the loss rate. The effective Hamiltonian with the non-Hermitian term neglects, in comparison with the Lindblad master equation, the fluctuation term $2\kappa a \rho a^\dagger$. A more sophisticated

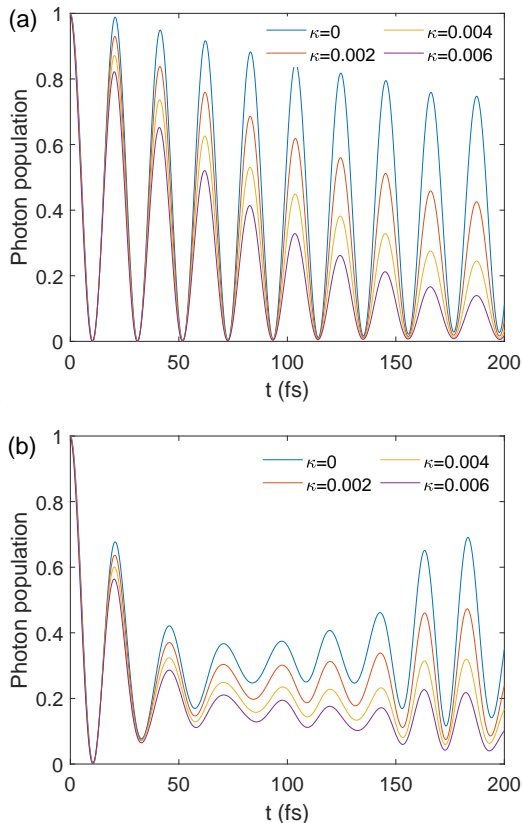


Figure 5. The photon-mode population dynamics with the finite inverse lifetimes $\kappa = 0$ eV, 0.002 eV, 0.004 eV, and 0.006 eV for (a): $\lambda = 0.1$ and (b): $\lambda = 0.4$. The other parameters are set by $\omega_R = 0.1$ eV, $N = 10$, $\omega_c = \omega_n = 1$ eV, and $\Omega = 0.5$.

scheme includes the coupling between the cavity mode and the environmental modes (namely, the Gardiner-Collett interaction Hamiltonian), characterized by a continuum spectral density. This Hamiltonian can be rigorously derived from the QED first-principles. It has been used to investigate polariton quantum dynamics in a dissipative cavity [25]. By constructing an effective non-Hermitian Hamiltonian or employing spectral discretization techniques, the time-dependent variation method with the mD2 Ansatz can be applied to account for dissipation scenarios.

For a nonzero cavity loss rate, both the upper and lower polariton states experience a depletion of their population, transferring it to the ground state. This loss of the excited state population typically diminishes the capacity of the system to undergo reactions on excited surfaces.

The photon population evolutions $\langle D_2^M(t) | \hat{a}^\dagger \hat{a} | D_2^M(t) \rangle$ for different cavity loss parameters κ and qubit-phonon couplings λ are plotted in Fig. 5. As the cavity loss increases, the photon population gradually decreases. Due to the finite lifetimes ($\kappa \neq 0$), the population decays to zero in the long-time limit. The bright-state energy gap for TC model is $\epsilon = \sqrt{(\omega_c - \omega_0)^2 + 4\omega_R^2} = 2\omega_R$, which

determines the oscillation period $2\pi/2\omega_R \sim 20.7$ fs of the photon population. As a comparison, for the case of weaker qubit-phonon coupling in HTC model as shown in Fig. 5(a), we can still observe the regular 20.7 fs periodic oscillations. For $\lambda = 0.4$, the phonon-qubit coupling significantly reduces amplitudes of these oscillations, as shown in Fig. 5(b). The stronger qubit-phonon coupling quenches Rabi oscillations, due to the increasing number of quantum states participating in the HTC dynamics. It is worth mentioning that a partial recurrence of photon population occurs after 150fs. We attribute it to the limited number of discrete phonon modes in the model. In addition, the period of Rabi oscillations has a small increment for a stronger phonon-qubit coupling in Fig. 5(b). Hence the renormalization Rabi frequency is slightly reduced by the qubit-phonon coupling.

IV. CONCLUSION

In this work, by employing the mD2 Ansatz, we have successfully carried out numerically “exact” simulations of various of non Hermitian quantum systems. For the non-Hermitian dissipative Landau-Zener transitions, we have predicted the logarithmic correspondence between the unnormalized population and the strength of non-Hermiticity for both single mode and multi mode scenarios, as the mD2 results coincide with that obtained via the TDSE. For the non-Hermitian, multi-mode JC model, we have found exact overlapping of the excited-state population calculated by mD2 Ansatz and the numerically exact approaches. Lastly, for the HTC model, we have demonstrate that the mD2 Ansatz can also handle Hermitian systems with non-Hermitian additions that serve as a phenomenological description of realistic experiments.

Beyond the three systems studied in this work, there are myriad other applications of mDA to non-Hermitian systems. As demonstrated in this work, mDA calculations are capable of providing phenomenological descriptions in non-Hermitian physics. It also serves as a powerful numerical apparatus to deal with complex many-body dynamics in non-Hermitian systems. The investigation of these systems could provide deeper insights into a range of intriguing phenomena, including non-Hermitian skin effects, non-Hermitian excited-state dynamics, and non-Hermitian evolution of quantum photonics systems. Additionally, since the mDA approach enables direct time-dependent calculations for non-Hermitian systems, it offers a convenient tool for exploring non-Hermitian spectral topology[53].

ACKNOWLEDGMENTS

The authors thank Lu Wang, Qinghu Chen, and Chenlin Ma for useful discussion. M. F. G. acknowledges support from the National Natural Science Foundation of China (Grant No. 22373028). Support from the Sin-

gapore Ministry of Education Academic Research Fund Tier 1 (Grant Nos. RG87/20 and RG2/24) is also gratefully acknowledged.

AUTHOR DECLARATIONS

Conflict of Interest

The authors have no conflicts to disclose.

DATA AVAILABILITY

The data that support the findings of this study are available from the corresponding author upon reasonable request.

Appendix: Derivation of Norm Decay in Non-Hermitian Hamiltonian Systems

We begin with a general non-Hermitian Hamiltonian

$$\hat{H} = \hat{H}_0 - i\hat{\Gamma} \quad (\text{A.1})$$

where \hat{H}_0 is Hermitian ($\hat{H}_0^\dagger = \hat{H}_0$), and $\hat{\Gamma}$ is a Hermitian, positive semi-definite operator ($\hat{\Gamma}^\dagger = \hat{\Gamma}$, $\langle \Psi(t) | \hat{\Gamma} | \Psi(t) \rangle > 0$) is responsible for the dissipative effects.

The TDSE is given by

$$i \frac{d}{dt} |\Psi(t)\rangle = \hat{H} |\Psi(t)\rangle \quad (\text{A.2})$$

The norm of the wavefunction is defined as

$$N(t) = ||\Psi(t)||^2 = \langle \Psi(t) | \Psi(t) \rangle \quad (\text{A.3})$$

Taking the time derivative of $N(t)$:

$$\frac{d}{dt} N(t) = \frac{d}{dt} \langle \Psi(t) | \Psi(t) \rangle = \left(\frac{d}{dt} \langle \Psi(t) | \right) |\Psi(t)\rangle + \langle \Psi(t) | \frac{d}{dt} |\Psi(t)\rangle \quad (\text{A.4})$$

Using the adjoint form of Eq. (A.2), we have

$$\left(\frac{d}{dt} \langle \Psi(t) | \right) = i \langle \Psi(t) | \hat{H}^\dagger \quad (\text{A.5})$$

Substituting this into Eq. (A.4), we get

$$\frac{d}{dt} N(t) = i \left(\langle \Psi(t) | \hat{H}^\dagger | \Psi(t) \rangle - \langle \Psi(t) | \hat{H} | \Psi(t) \rangle \right) \quad (\text{A.6})$$

Applying the condition

$$\hat{H} - \hat{H}^\dagger = (\hat{H}_0 - i\hat{\Gamma}) - (\hat{H}_0 + i\hat{\Gamma}) = -2i\hat{\Gamma} \quad (\text{A.7})$$

We obtain

$$\frac{d}{dt} N(t) = -2 \langle \Psi(t) | \hat{\Gamma} | \Psi(t) \rangle < 0 \quad (\text{A.8})$$

Thus, the total population decays with time.

-
- [1] Ashida, Y.; Gong, Z.; Ueda, M. Non-Hermitian Physics. *Adv. Phys.* **2020**, *69*, 249-435.
 - [2] Kawabata, K.; Shiozaki, K.; Ueda, M.; Sato, M. Symmetry and Topology in Non-Hermitian Physics. *Phys. Rev. X* **2019**, *9*, 041015.
 - [3] Bergholtz, E. J.; Budich, J. C.; Kunst, F. K. Exceptional Topology of Non-Hermitian Systems. *Rev. Mod. Phys.* **2021**, *93*, 015005.
 - [4] Wang, C.; Fu, Z.; Mao, W. Non-Hermitian optics and photonics: from classical to quantum *Adv. Opt. Photonics* **2023**, *15*, pp. 442-523.
 - [5] Shen, H.; Zhen, B.; Fu, L. Topological band theory for non-Hermitian Hamiltonians. *Phys. Rev. Lett.* **2018**, *120*, 146402.
 - [6] Kawabata, K.; Bessho, T.; Sato, M. Classification of exceptional points and non-Hermitian topological semimetals. *Phys. Rev. Lett.* **2019**, *123*, 066405.
 - [7] Hu, H.; Zhao, E. Knots and non-Hermitian Bloch bands. *Phys. Rev. Lett.* **2021**, *126*, 010401.
 - [8] Zhang, Z. X.; Huang, R.; Qi, L.; Xing, Y.; Zhang, Z. J.; Wang, H. F. Topological phase transition and eigenstates localization in a generalized non-Hermitian su-schrieffer-heeger model. *Ann. Phys.* **2021**, *533*, 2000272.
 - [9] Longhi, S. Non-Hermitian topological phase transitions in superlattices and the optical Dirac equation. *Opt. Lett.* **2021**, *46*, 4470-4473.
 - [10] Ao, Y.; Hu, X.; You, Y.; Lu, C.; Fu, Y.; Wang, X.; Gong, Q. Topological phase transition in the non-Hermitian coupled resonator array. *Phys. Rev. Lett.* **2020**, *125*, 013902.
 - [11] Longhi, S. Non-Hermitian topological phase transition in PT-symmetric mode-locked lasers. *Opt. Lett.* **2019**, *44*, 1190-1193.
 - [12] Longhi, S. Topological phase transition in non-Hermitian quasicrystals. *Phys. Rev. Lett.* **2019**, *122*, 237601.
 - [13] Zhao, X. L.; Chen, L. B.; Fu, L. B.; Yi, X. X. Topological phase transition of non-Hermitian crosslinked chain. *Ann. Phys.* **2020**, *532*, 1900402.
 - [14] Kunst, F. K.; Edvardsson, E.; Budich, J. C.; Bergholtz, E. J. Biorthogonal bulk-boundary correspondence in non-Hermitian systems. *Phys. Rev. Lett.* **2018**, *121*, 026808.
 - [15] Zirnstein, H.-G.; Refael, G.; Rosenow, B. Bulk-boundary correspondence for non-Hermitian Hamiltonians via green functions. *Phys. Rev. Lett.* **2021**, *126*, 216407.
 - [16] Sarkar, R.; Hegde, S. S.; Narayan, A. Interplay of disorder and point-gap topology: chiral modes, localization, and non-Hermitian Anderson skin effect in one dimension. *Phys. Rev. B* **2022**, *106*, 014207.

- [17] Claes, J.; Hughes, T. L. Skin effect and winding number in disordered non-Hermitian systems. *Phys. Rev. B* **2021**, *103*, L140201.
- [18] Kunst, F. K.; Dwivedi, V. Non-Hermitian systems and topology: a transfer-matrix perspective. *Phys. Rev. B* **2019**, *99*, 245116.
- [19] Ochiai, T. Non-Hermitian skin effect and lasing of absorbing open-boundary modes in photonic crystals. *Phys. Rev. B* **2022**, *106*, 195412.
- [20] K. Zhang, Z. Yang, C. Fang, *Nat. Commun.* **2022**, *13*, 2049.
- [21] Farsal, Farhad H. M. *Theory of multiphoton processes*; Springer, New York, 1980
- [22] Goldman, N.; Dalibard, J. Periodically Driven Quantum Systems: Effective Hamiltonians and Engineered Gauge Fields *Phys. Rev. X* **2014**, *4*, 031027.
- [23] El-Ganiny, R.; Makris, K.; Khajavikhan, M.; Mussli-mani, Z. H.; Rotter, S.; Christodoulides, D. N. Non-Hermitian Physics and PT Symmetry. *Nat. Phys.* **2018**, *14*, 11.
- [24] Moiseyev, N. *Non-Hermitian Quantum Mechanics*; Cambridge University Press: Cambridge, 2011.
- [25] Mandal, A.; Taylor, M. A.; Weight, B. M.; Koessler, E. R.; Li, X.; Huo, P. Theoretical Advances in Polariton Chemistry and Molecular Cavity Quantum Electrodynamics. *Chem. Rev.* **2023**, *123*, 9786-9879.
- [26] McTague, J.; Foley, J. J. Non-Hermitian Cavity Quantum Electrodynamics-Configuration Interaction Singles Approach for Polaritonic Structure with Ab Initio Molecular Hamiltonians. *J. Chem. Phys.* **2022**, *156*, 154103.
- [27] Fregoni, J.; Granucci, G.; Coccia, E.; Persico, M.; Corni, S. Manipulating Azobenzene Photoisomerization through Strong Light-Molecule Coupling. *Nat. Commun.* **2018**, *9*, 4688.
- [28] Fregoni, J.; Granucci, G.; Persico, M.; Corni, S. Strong Coupling with Light Enhances the Photoisomerization Quantum Yield of Azobenzene. *Chem.* **2020**, *6*, 250-265.
- [29] Antoniou, P.; Suchanek, F.; Varner, J. F.; Foley, J. J. Role of Cavity Losses on Nonadiabatic Couplings and Dynamics in Polaritonic Chemistry. *J. Phys. Chem. Lett.* **2020**, *11*, 9063-9069.
- [30] Mauro, L.; Caicedo, K.; Jonusauskas, G.; Avriller, R. Charge-Transfer Chemical Reactions in Nanofluidic Fabry-Perot Cavities. *Phys. Rev. B* **2021**, *103*, 165412.
- [31] Koessler, E. R.; Mandal, A.; Huo, P. Incorporating Lindblad Decay Dynamics into Mixed Quantum-Classical Simulations. *J. Chem. Phys.* **2022**, *157*, 064101.
- [32] Torres-Sánchez, J.; Feist, J. Molecular Photodissociation Enabled by Ultrafast Plasmon Decay. *J. Chem. Phys.* **2021**, *154*, 014303.
- [33] Felicetti, S.; Fregoni, J.; Schnappinger, T.; Reiter, S.; de Vivie-Riedle, R.; Feist, J. Photoprotecting Uracil by Coupling with Lossy Nanocavities. *J. Phys. Chem. Lett.* **2020**, *11*, 8810-8818.
- [34] Davidsson, E.; Kowalewski, M. Simulating Photodissociation Reactions in Bad Cavities with the Lindblad Equation. *J. Chem. Phys.* **2020**, *153*, 234304.
- [35] Zhao, Y.; Sun, K.; Chen, L.; Gelin, M. The Hierarchy of Davydov's Ansätze and Its Applications. *WIREs Comput. Mol. Sci.* **2022**, *12*, e1589.
- [36] Zhao, Y. The Hierarchy of Davydov's Ansätze: From Guesswork to Numerically "Exact" Many-Body Wave Functions. *J. Chem. Phys.* **2023**, *158*, 080901.
- [37] Shen, K.; Sun, K.; Gelin, M. F.; Zhao, Y. Finite-Temperature Hole-Magnon Dynamics in an Antiferromagnet. *J. Phys. Chem. Lett.* **2024**, *15*, 447-453.
- [38] Sun, K.; Shen, K.; Gelin, M. F.; Zhao, Y. Exciton Dynamics and Time-Resolved Fluorescence in Nanocavity-Integrated Monolayers of Transition-Metal Dichalcogenides. *J. Phys. Chem. Lett.* **2022**, *14*, 221-229.
- [39] Shen, K.; Sun, K.; Gelin, M. F.; Zhao, Y. Cavity-Tuned Exciton Dynamics in Transition Metal Dichalcogenides Monolayers. *Materials* **2024**, *17*, 4127.
- [40] Zheng, F.; Shen, Y.; Sun, K.; Zhao, Y. Photon-Assisted Landau-Zener Transitions in a Periodically Driven Rabi Dimer Coupled to a Dissipative Mode. *J. Chem. Phys.* **2021**, *154*, 044101.
- [41] Zhang, L.; Gelin, M. F.; Zhao, Y. Dissipative Landau-Zener transitions in a three-level bow-tie model: accurate dynamics with the Davydov multi-D2 Ansatz. *Adv. Quant. Tech.* **2024**, *7*, 2300285.
- [42] Sun, K.; Huang, Z.; Gelin, M. F.; Chen, L.; Zhao, Y. Monitoring of singlet fission via two-dimensional photon-echo and transient-absorption spectroscopy: Simulations by multiple Davydov trial states. *J. Chem. Phys.* **2019**, *151*, 114102.
- [43] Xianqi Tong, Gao Xianlong, and Su-peng Kou, *Phys. Rev. B* **2023**, *107*, 104306.
- [44] Z. Y. Liao, X. D. Zeng, S.-Y. Zhu, and M. S. Zubairy, *Phys. Rev. A* **2015**, *92*, 023806.
- [45] Z. Y. Liao, H. Nha, and M. S. Zubairy, *Phys. Rev. A* **2016**, *94*, 053842.
- [46] Z.-J. Ying, *Adv Quantum Technol.* **2024**, *7*, 2400053.
- [47] Kramer, P.; Saraceno, M. Geometry of the Time-Dependent Variational Principle in Quantum Mechanics. Springer Berlin Heidelberg: Berlin, Heidelberg, 1981.
- [48] Broeckhove, J.; Lathouwers, L.; Kesteloot, E.; Van Leuven, P. On the Equivalence of Time-Dependent Variational Principles. *Chem. Phys. Lett.* **1988**, *149*, 547-550.
- [49] Yuan, X.; Endo, S.; Zhao, Q.; Li, Y.; Benjamin, S. C. Theory of Variational Quantum Simulation. *Quantum* **2019**, *3*, 191.
- [50] K. Sun, C. Dou, M. F. Gelin, Y. Zhao, *J. Chem. Phys.* **2022**, *156*, 024102.
- [51] K. Sun, M. F. Gelin, Y. Zhao, *J. Phys. Chem. Lett.* **2022**, *13*, 4090-4097.
- [52] K. Sun, M. F. Gelin, Y. Zhao, *J. Phys. Chem. Lett.* **2022**, *13*, 4280-4288.
- [53] N. Okuma, M. Sato, *Annu. Rev. Condens. Matter Phys.* **2023**, *14*, 83-107.